Review Article

Matthias Baier*, Jan Sparbert and Cornelius Neumann

Novel refractive LiDAR sensor based on a variable lens pair prism

https://doi.org/10.1515/aot-2018-0054
Received October 8, 2018; accepted February 16, 2019; previously published online March 23, 2019

Abstract: We present a new type of Light Detection And Ranging (LiDAR) sensor based on a variable lens pair prism. This system combines the principles of macro- and microscanners to exploit the advantages and eliminate most of the disadvantages of both system types. We describe the concept of this new LiDAR sensor and examine the system performance by simulation. Afterwards, we investigate the spot shape and beam profile with respect to the main system parameters such as the gap between lenses, the deflection angle, and the measurement distance. Furthermore, we present solutions to optimize the variable lens pair prism to achieve an ideal spot shape and beam profile in the entire field of view (FoV).

Keywords: laser scanner; LiDAR; prism; refractive optics.

1 Introduction

In addition to established sensors such as cameras, radar, or ultrasonic sensors, Light Detection And Ranging (LiDAR) sensors become increasingly important in the context of highly automated driving (HAD) and autonomous driving. Most current LiDAR sensors are based on at least one rotating or oscillating active component [1]. Macroscanners usually consist of a rotor including one or more lasers and/or detectors to scan the field of view (FoV). In contrast, microscanners deflect one or few laser beams with an oscillating mirror. Another type of LiDAR sensor uses passive components such as mirrors on a rotor to generate one scanning direction. All existing systems have different limitations concerning their performance.

In terms of redundancy and sensor fusion, LiDAR sensors are intended to be an inherent component of the sensor setup in HAD vehicles. For distance and velocity determination, LiDAR uses the principle of time-of-flight (ToF) measurement. This means the system emits a laser pulse and measures the time until a detector in the LiDAR sensor receives a reflected or scattered signal. Using the speed of light, the information about the elapsed time is converted into a distance [2]. There are two different types of LiDAR sensors: flash systems that illuminate the entire FoV at once [3] and scanning systems with a few laser beams that are moved across the FoV. The area observed by a scanning LiDAR sensor [4], the FoV, is limited by

$$\mathrm{FoV_h} \cdot \mathrm{FoV_v} = \frac{1}{fps \cdot t_{\mathrm{ToF}}} \cdot \delta_{\mathrm{h}} \cdot \delta_{\mathrm{v}} \tag{1}$$

due to time t_{ToF} for maximum measurement distance, resolution δ_{h} and δ_{v}, and frame rate *fps*.

Flash LiDAR sensors require very high illumination power to simultaneously achieve both a significant measurement distance and a large FoV. Lasers that provide sufficient illumination power are currently still too expensive and too large for automotive LiDAR sensors. For this reason, most of the LiDAR sensors and prototypes developed so far utilize, at least in part, a scanning principle.

In general, scanning systems are subdivided in two main groups: macroscanners and microscanners. The essential characteristic of a macroscanner is the combination of a rotating and a static part (rotor-stator system). There are different types of macroscanners, dependent on the placement of active components such as emitter and receiver. Usually, macroscanners with active components on the rotor have high rotating masses and power losses due to wireless energy transfer. However, scans of a very large horizontal FoV (up to 360°) are possible. In addition to that, only a limited amount of lasers and/or detectors

***Corresponding author: Matthias Baier,** Robert Bosch GmbH, Chassis Systems Control, Herrenwiesenweg 24, 71701 Schwieberdingen, Germany; and Karlsruher Institut für Technologie, Lichttechnisches Institut, Engesserstraße 13, 76131 Karlsruhe, Germany, e-mail: Matthias.Baier2@bosch.com
Jan Sparbert: Robert Bosch GmbH, Chassis Systems Control, Herrenwiesenweg 24, 71701 Schwieberdingen, Germany
Cornelius Neumann: Karlsruher Institut für Technologie, Lichttechnisches Institut, Engesserstraße 13, 76131 Karlsruhe, Germany

can be placed on the rotor, which limits vertical resolution [5–8].

Scanning systems with all active components on the stator use a passive component, e.g. a mirror, on the rotor to deflect the laser beam into the FoV. This arrangement enables reduction of the rotating mass and power losses. The rotation axis of the mirror can be orthogonal, parallel, or tilted with respect to the emitting beam direction. In all cases, there are only a few lasers and/or detectors aligned to the mirror and thus, the vertical resolution is discrete.

For mirror-based scanners with an orthogonal design, the main scan direction cannot be used because the mirror reflects the incoming beam back towards the laser. As a result, the orthogonal setup is optimized for a mirror rotation position of 45°. Because of the maximum reflection angle and the described tilted setup, a horizontal FoV from 15° to 165° is possible. On the downside, the optical path is also used to deflect the backscattered beam on the detector. Thus, the receiving aperture is limited by the projected area of the mirror. In other words, the receiving aperture depends on the rotational position of the mirror and has an asymmetric relation over the deflection range. Another aspect is the rotation speed combined with the beam reflection resulting in a doubled angular velocity of the scan. This increased angular velocity results either in the necessity of a high pulse repetition frequency of the laser or a reduced horizontal resolution [9–13].

On the contrary, a parallel setup scans with the angular velocity of the rotation, and the horizontal FoV is unlimited (360°). The most significant disadvantage of this setup is a varying vertical FoV due to the rotation. For example, a vertical line would rotate around its center during one rotation of the rotor and become a horizontal line for rotation angles of 90° and 270° [14, 15]. Setups with other tilt angles combine the properties of the parallel and orthogonal setups.

The second category of scanning LiDAR sensors are microscanners that use two-dimensional oscillating mirrors instead of rotor-stator combinations. The main advantage of these systems is a very high vertical resolution. However, the maximum deflection angles of micro-mirrors limit the vertical and horizontal FoV. In comparison with macroscanners, only the horizontal FoV (about 50°–60°) is significantly smaller [16, 17]. Unlike all setups mentioned above, micro-mirror systems are restricted in terms of the beam size. Two effects cause this limitation: first, the very small mirror size and, second, the impossibility to perform a beam expansion without reducing the scanning angle or losing the continuous vertical scanning capability. A small beam causes either a reduced measurement range or a non-eye-safe system.

2 Concept of a LiDAR sensor based on a variable lens pair prism

The fundamental approach is similar to the orthogonal setup of a macroscanner described above [9–13]. The main difference in the setup is a lens pair that is used instead of the mirror. The lens pair has the same purpose as the rotating mirror, i.e. to deflect the laser beam in the horizontal FoV. However, in this setup, the main scanning direction is available. As before, beam deflection in the second direction is independent of the horizontal deflection, whereby, various concepts for the vertical scan are conceivable. In particular, a one-dimensionally oscillating mirror (see (3) in Figure 1) is the concept of choice in the lens pair-based LiDAR sensor. The combination of an oscillating mirror and a lens pair enables sufficient horizontal FoV and high vertical resolution.

As one might expect from Figure 1, at large angles of rotation, there is a reflection on the plane side of the rotating lens (4). This reflected beam leaves the sensor as a false signal, but is previously diverged by the static lens (5). Even with a highly reflective object at a short distance, the potential back reflex is of very low intensity. In addition, an appropriate coating on the lens surfaces can further reduce the false signal.

In the receiving path, the backscattered light passes through the lens pair first. Hence, the deflection generated during the transmission is inverted (see Figure 1B). Thus, after passing the lens pair, the received light propagates almost without horizontal angle, i.e. parallel to the optical axis. Similar to the orthogonal setup [9–13], the center of the receiving path is obscured, but in this case by the oscillating mirror. However, as the backscattered light floods the entire lens diameter and is focused on the detector, the received signal is only attenuated in proportion to the area covered. As shown in Figure 1C, the vertical scan direction is not reversed but focused on different segments of a detector array. Accordingly, the transmitting and receiving paths use the same horizontal axis but different vertical axes. Therefore, the entire setup can be described as semi-coaxial.

In general, the lens pair consists of two lenses, where one is positioned on the rotor (rotating lens, RL, (4) in Figure 1) and the other one on the stator (static lens, SL, (5) in Figure 1). The lenses are arranged opposite each other so that they form a prism-like optic together. In order to enable unrestricted rotation of the RL along the SL, the facing surfaces of the lenses need to have a similar curvature. Additionally, the RL rotates around the center of its curved surface. According to these boundary

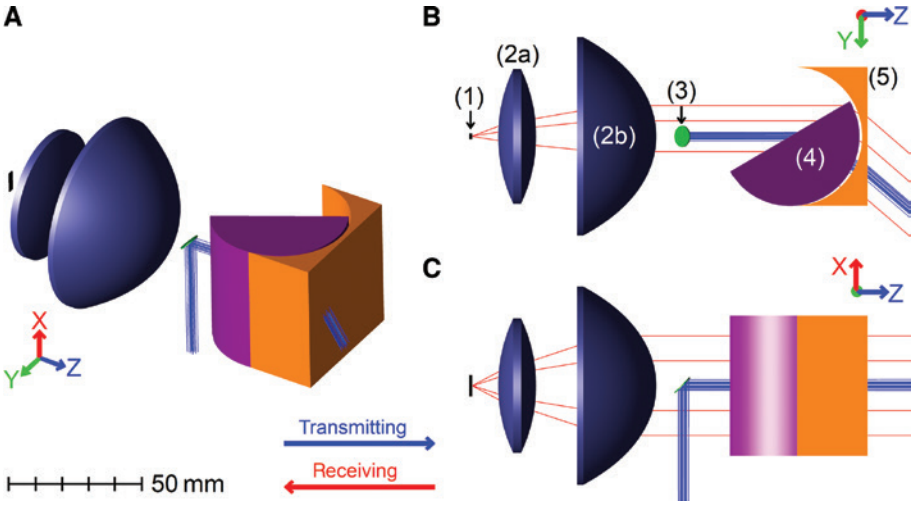

Figure 1: Schematic drawing of a LiDAR sensor based on a lens pair. (A) Perspective overview: the main components such as detector (1), two focusing lenses (2a) and (2b), oscillating mirror (3), rotating lens (4), and static lens (5). (B) Top view: the horizontal deflection by the lens pair (C) Side view: the receiving path in the vertical direction.

conditions, the RL is plano-convex and the SL is plano-concave with the curved surfaces facing each other. To prevent possible contact, there has to be a gap between the RL and the SL. In principle, both lenses can have a spherical curved surface, but cylindrical lenses are preferred because they have almost no effect on the vertical scan.

The rotation of the RL results in a varying angle between the planar surfaces of the RL and the SL. Simplified, this angle can be interpreted as the apex angle of a prism. Thus, the lens pair can be described as a prism with variable apex angle or, in short form, as a variable lens pair prism (VLPP). Because of the variable apex angle, a nonlinear relation between the rotation angle and the deflection angle results for the VLPP. There are two additional parameters, the refractive index of the lens material and the gap between the lenses (LG), influencing the angle relation. In Figure 2, the angle relation for lenses made of borosilicate glass (BK7) with a refractive index of 1.52 for light at the wavelength 532 nm is shown. The blue graph displays the simplified prism relation, while the red graph represents the real VLPP with an LG of 1 mm.

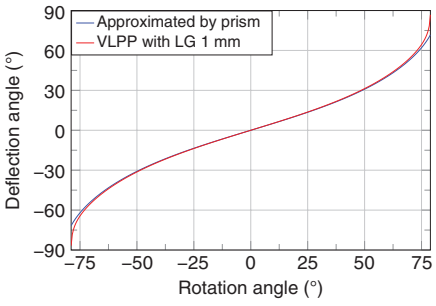

Figure 2: Relation between rotation angle and deflection angle approximated by a prism (blue graph) and calculated for a VLPP with a gap of 1 mm between the lenses (red graph).

As indicated in Figure 2, the approximation of the VLPP by a prism with varying apex angle is acceptable for the VLPP with small lens gaps and rotation angles up to 60°.

A valuable side effect of the nonlinearity in the angle relation of the VLPP is the reduced angular velocity, slower than the rotation speed, in the center of the horizontal scan. From this, more time for scanning in this part of the FoV becomes available, and hence, a higher resolution can be achieved.

In the following sections, the investigation of the operating principle of the VLPP is described, focusing mainly on the transmitting path and the properties of the system in the measurement range.

3 Simulation setup to observe the spot shape generated by a VLPP

The spot shape generated by the VLPP is of particular interest for optimizing the LiDAR sensor in terms of system properties and performance. Thus, a setup for an optical simulation program (in this case, OpticStudio [18]) is introduced, by which the spot parameters can be simulated. In the environment of the simulation program, only geometrically optical calculations are performed. Diffraction effects can be neglected due to the macroscopic structure of the system.

In order to interpret the simulated data, the light source used must be specified first. As most lasers have a Gaussian mode at their output, in the simulation program, a Gaussian source with a full divergence of 0.15°, 1 W emitted power, and one million rays is modeled. The beam radius, evaluated for the $1/e^2$ restriction of the intensity distribution in a Gaussian beam before passing the VLPP, is 2.25 mm.

The Gaussian source illuminates a VLPP consisting of two lenses, where one can be rotated around the center of its curvature. The RL has a 50.8 mm × 53 mm plane surface and a curved surface with a radius of 26.35 mm. The counterpart is the SL with a plane surface of the same dimensions, whereas the radius of the curved surface is –26.35 mm. Regarding the curved surface, the lenses fit together completely. In addition, the SL is 2 mm thick at the thinnest point.

To observe the spot shape and profile over the entire horizontal FoV, the three main influencing parameters are varied. To limit the simulation effort, the deflection angle δ, measurement distance z, and LG are alternatingly adjusted in discrete steps. The deflection angle is indirectly configured by rotation of the RL in a way that simulations can be taken every 10° from 0° to 60° deflection. Corresponding to the deflection angles, detector screens are positioned in the FoV with measurement distances of 1 m, 5 m, 10 m, 50 m, and 100 m with respect to the exit point of the beam on the SL. Observing these screens during ray trace simulation allows to record cross sections or rather spot profiles of the transmitted beam. An important parameter of the detector screen definition is the amount of pixels it should have. This, in combination with the amount of simulated rays, always results in discrete spot profile resolutions. On the other hand, the amount of pixels scales directly with the simulation time and the data volume. As a compromise, 1000 × 1000 pixels are used most of the time. Because of beam divergence and other effects caused by the VLPP, screen sizes have to be reviewed and, if necessary, adjusted for every measurement distance, LG, and deflection angle.

The third parameter is the gap between the lenses needed to avoid contact. This variable size is a design parameter of the VLPP. Therefore, the impact of the LG on the spot shape is investigated. The evaluated discrete steps of the LG are 0 mm, 0.1 mm, 0.5 mm, 1 mm, 1.5 mm, and 2 mm.

To compare the spot size at different measurement distances, a reference is needed. Therefore, the spot at the exit point is evaluated for every LG and deflection angle.

4 Interpreting spots by evaluation of simulated data

Data simulated with the setup described in Section 3 can be displayed in OpticStudio. Unfortunately, the evaluation of these data sets is very limited in the program environment. Only the visual interpretation of the spot profile can be performed reasonably easily. In order to derive relations between system parameters and their effect on system performance, the data sets of the spots have to be evaluated in detail. Therefore, several steps necessary to interpret the data are presented.

First, the data sets are read in succession to obtain the detector screen information. Here, the irradiance on each detector pixel as well as the size and number of pixels in both dimensions of the screen represent the most important basis for evaluation. Second, the spot profile can be interpreted based on the definition of a Gaussian beam. The centroid $\langle x_c(z)\rangle$ in the x direction is calculated for each spot according to

$$\langle x_c(z)\rangle = \frac{\int_{x_{min}}^{x_{max}} x \cdot \left(\int_{y_{min}}^{y_{max}} E(x,y,z)dy \right) dx}{\int_{x_{min}}^{x_{max}} \int_{y_{min}}^{y_{max}} E(x,y,z)dxdy}, \tag{2}$$

where x and y are the positions of the pixels on the detector screen, z is the measurement distance, and E is the irradiance of each pixel [19]. Because of the discrete detector screen resolution, the integrals are substituted by sums, which results in

$$\langle x_c(z)\rangle = \frac{\sum_{x_{min}}^{x_{max}} x \cdot \left(\sum_{y_{min}}^{y_{max}} E(x,y,z) \right)}{\sum_{x_{min}}^{x_{max}} \left(\sum_{y_{min}}^{y_{max}} E(x,y,z) \right)}. \tag{3}$$

Consequently, the variance $\langle x^2(z)\rangle$ in the x direction is given by

$$\langle x^2(z)\rangle = \frac{\sum_{x_{min}}^{x_{max}} (x - x_c(z))^2 \cdot \left(\sum_{y_{min}}^{y_{max}} E(x,y,z) \right)}{\sum_{x_{min}}^{x_{max}} \left(\sum_{y_{min}}^{y_{max}} E(x,y,z) \right)} \tag{4}$$

As the standard deviation is the square root of the variance and the beam radius r of a Gaussian beam is defined as twice the standard deviation, we obtain for the x direction

$$r_x = 2 \cdot \sqrt{\langle x^2(z)\rangle} \tag{5}$$

Centroid, variance, and beam radius in the y direction can be determined analogous to Eqs. (2)–(5). The radius and centroid for both directions are sufficient to draw the spot ellipse thus indirectly fitted (see an example in Figure 3).

As shown in Figure 3, the calculation described allows an interpretation of the cross section through a Gaussian beam. However, a reference is necessary for a meaningful evaluation of the generated spots. As the influence of the VLPP is investigated, the reference of the system with exception of the deflection angle is an unchanged propagating beam. For the calculation of the reference spot radius at various measurement distances z, we use

$$r_{x;ref} = r_{x;0} + z \cdot \tan(\theta_{div}) \tag{6}$$

with the spot radius $r_{x;0}$ at the exit point on the SL and the beam divergence θ_{div} in the x direction. Analogously to Eq. (5), the reference spot radius in the y direction is determined. Because of the positioning of the detector screens described in Section 3, the centroid of the reference spot is always in the center or rather the origin of the detector screen. Thus, by evaluating the centroid of the simulated spots, their positional uncertainty can be determined.

Further criteria for comparison of the simulated spot and the reference spot are their overlap area, the optical power on this area, and the shape conformity of the spots. The shape conformity is evaluated by comparing the length of the semi-axes of the spot to the length calculated in Eq. (6). In order to obtain a reliable statement, all criteria are set in relation to the reference spot properties.

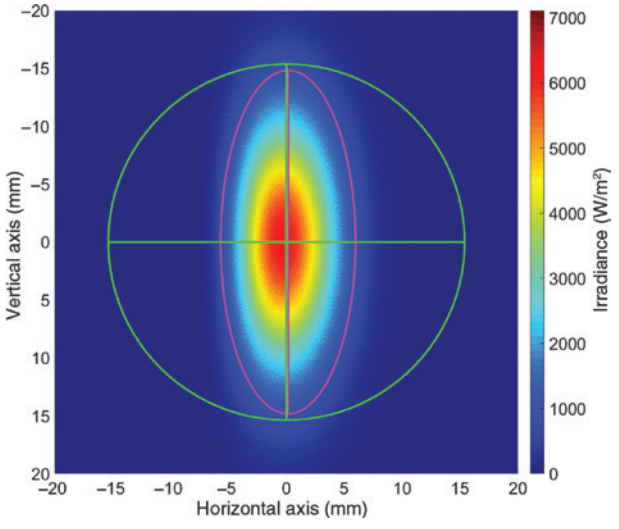

Figure 3: Example of a spot profile by means of its irradiance distribution with the fitted ellipse (magenta) and the reference spot (green). This diagram represents a spot for total transmitting power of 1 W, a measurement distance of 10 m, a LG of 1 mm, and a deflection angle of 10°.

Thus, we get values that represent the ratio for how well the overlap area corresponds to the area of the reference spot (area ratio). In the same way, it is determined how much of the optical power of the reference spot hits the overlap area (optical power ratio) and how well the lengths of the semi-axes of the simulated spot correspond to the semi-axes of the reference spot (shape conformity).

5 Influences of system parameters on spot shape

The first series of simulations clarifies the influence of the deflection angle on the spot shape and profile. Therefore, the gap between the lenses is set to 0 mm. Figures 4 to 6 show the influence of the deflection angle on centroid,

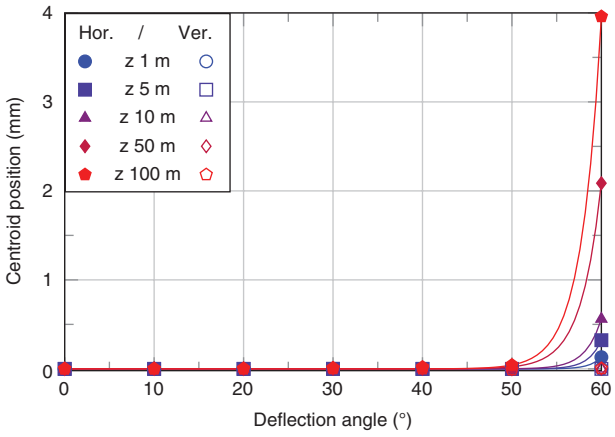

Figure 4: Position of the centroid in the horizontal and vertical direction over the deflection angle at different measurement distances. Besides the simulation results (marks), fitted exponential curves are shown as solid lines.

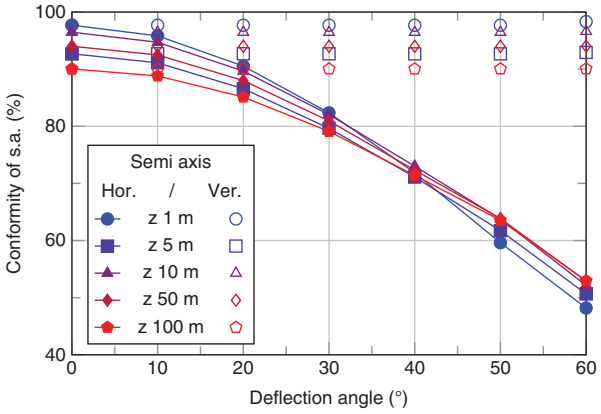

Figure 5: Conformity of semi-axes of the simulated spot ellipse to the reference spot ellipse over the deflection angle at different measurement distances.

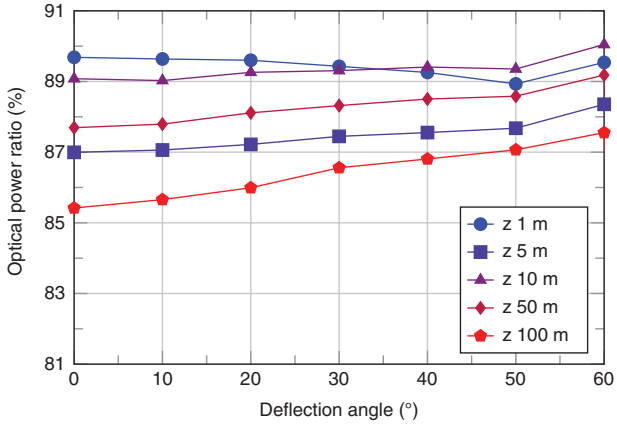

Figure 6: Optical power ratio of overlap area to reference spot over the deflection angle at different measurement distances.

shape conformity, and optical power ratio for different measurement distances. As described in Section 3, the deflection angle and measurement distance are varied in discrete steps. To get a visual impression of the influence of these parameters in some of the graphs, lines are drawn between the simulation results.

As presented in Figure 4, deflection angles of up to 50° have almost no effect on the position of the centroid. In addition, only the horizontal position of the centroid is affected because the VLPP generates the horizontal deflection angle and does not significantly change vertical beam propagation. Deflection angles greater than 50° yield to a shift of the centroid in a continuous way. This can be explained by the eccentricity of the rotating lens. The thickness of the RL used in the simulations is smaller than the radius of curvature, which leads to an eccentricity of the plane surface of the RL relative to the center of rotation. Therefore, the RL rotates out of the optical path of the laser beam. At deflection angles greater than 50°, a part of the laser beam misses the RL and is not deflected. This part of the laser beam is absent in the spot evaluation, whereby the calculation of the centroid and the semi-axes is affected. The centroid shifts to values greater than zero, and the semi-axes become slightly shorter than for a complete Gaussian beam.

As suggested by theoretical considerations, the simulation proves that the deflection angle generated by the VLPP only influences the conformity of the horizontal spot shape (see Figure 5).

Figure 6 shows that despite the reduced spot size, the optical power ratio remains constant for all measurement distances and deflection angles. This means that with increasing deflection angle, the optical power is concentrated on a smaller area. In other words, the beam becomes an oblate ellipse in the horizontal direction. This behavior originates in the prism-like setup of the VLPP. While passing, prisms deform a round beam to an elliptical beam depending on the total deflection. The greater the deflection angle, the more the beam is deformed.

Further simulation series allow for the evaluation of the influences caused by the gap between the two lenses at different deflection angles and measurement distances. Based on a representative example with a measurement distance of 10 m, the essential consequences of the necessary LG are described below.

As before, only the horizontal position of the centroid is influenced by the VLPP (see Figure 7). Because of the asymmetric gap between the lenses, the influence on the spot shape is also not symmetric, resulting in various spot shapes and, consequently, a shift of the centroid. This effect gains impact with increasing deflection angle and increasing LG. Furthermore, the position of the centroid is unpredictable and may vary widely depending on the simulated setup (see deflection angle of 60° in Figure 7). This suggests that the calculation described in Section 4 is not appropriate for every spot shape.

Considering the conformity of the spot shape presented in Figure 8, a minimum in the horizontal direction is identifiable for each deflection angle depending on the LG. Additionally, with increasing LG, the conformity decreases before the minimum and rises afterward. This behavior indicates a focal length, which shifts according to the LG or the deflection angle. The reason for this focal length is due to a parasitic air lens caused by the gap between the lenses. In the simulated setup, the radius of curvature of both lenses is identical, whereby the gap between the lenses is constant in the z direction. Therefore, the radial gap respective to the rotation center is not constant, which leads to a variation of the parasitic air lens with the deflection angle. Accordingly, the air lens

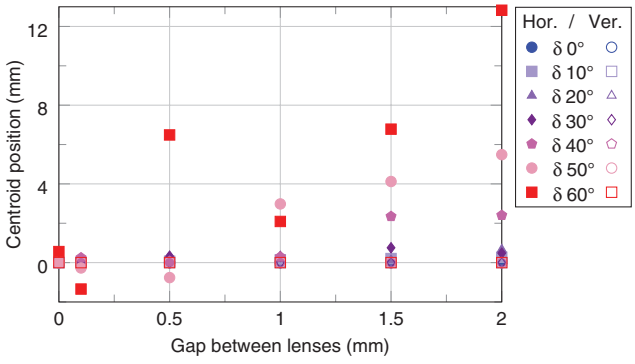

Figure 7: Position of the centroid in the horizontal and vertical directions over the gap between the lenses at different deflection angles.

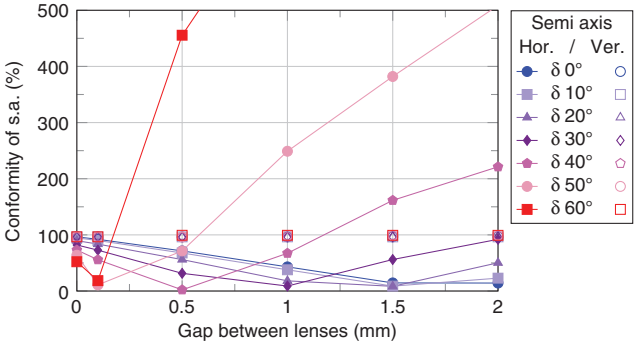

Figure 8: Conformity of semi-axes of the simulated spot ellipse to the reference spot ellipse over the gap between the lenses at different deflection angles.

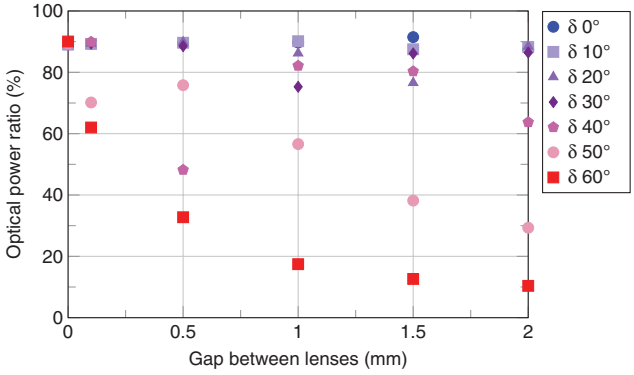

Figure 10: Optical power ratio of overlap area to reference spot over the gap between the lenses at different deflection angles.

focal length varies with the deflection angle and with the gap between the lenses on the optical axis.

The area ratio shown in Figure 9 confirms the effect of a parasitic air lens. The smaller the LG and the greater the deflection angle, the shorter the air lens focal length.

Figure 10 shows that the power ratio remains between 80% and 100% as long as the simulated spot is smaller or equal to the reference spot. However, all optical power affects a small area if the spot is focused. This means that very high irradiances can occur due to the focal length of the air lens. To ensure the eye safety of the entire sensor, the focused spot would limit the permissible laser power emitted. Another effect of the parasitic air lens can be seen in Figure 10 for deflection angles of 50° and 60°. The high divergence caused by a short focal length of the air lens leads to very large spots. Thus, the optical power spreads on this large area, and only a small fraction of the optical power hits the area of the reference spot. Furthermore, the horizontal resolution is affected by the inhomogeneous spot sizes.

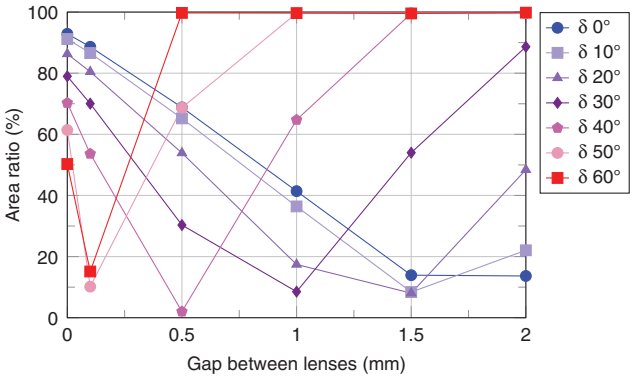

Figure 9: Area ratio of overlap area from simulated spot and reference spot to reference spot area over the gap between the lenses at different deflection angles.

According to the simulation results, the influences of the VLPP on the spot shape and the spot profile are not negligible. Hence, the next section introduces a few system adjustments by which the characteristics of the VLPP can be optimized.

6 Correcting spot shape by adjusting system parameters

In order to obtain better system characteristics for large deflection angles, the geometry of the RL is changed. One approach is to increase the thickness so that the cross section corresponds to a semicircle. With this configuration, due to geometrical considerations, the maximum deflection angles should be achievable without cutting off the laser beam. Additionally, the radius of the SL is adjusted to create a radially constant gap. As in Section 5, the LG is varied in discrete steps, but for each step, the radius of curvature r_{SL} of the SL is modified according to

$$r_{SL} = -r_{RL} + d_{LG}, \tag{7}$$

where r_{RL} is the radius of curvature of the RL, and d_{LG} is the gap between the lenses on the optical axis. The radially constant gap influences the relation of the deflection angle to the rotation angle. This adjustment makes the relation independent of the LG.

The simulation of this adjusted VLPP demonstrates better results for deflection of a laser beam. For example, the centroid of the simulated spots always hits the center of the reference spots (see Figure 11). Only for large deflection angles, a shift of the centroid can be identified in the horizontal direction. This result originates from the

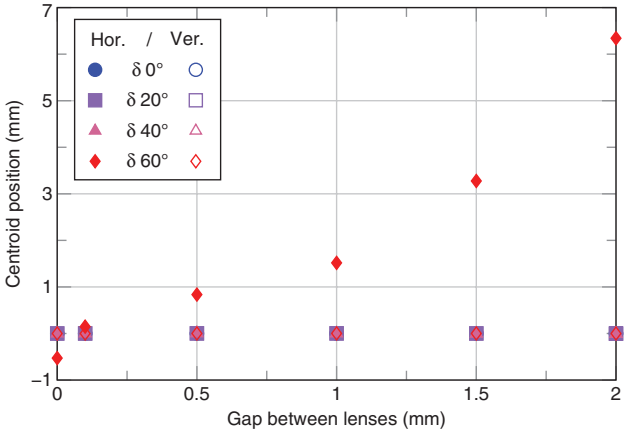

Figure 11: Position of the centroid in the horizontal and vertical direction over the gap between the lenses at different deflection angles. A VLPP with a semicircle RL and a radial constant gap between the lenses.

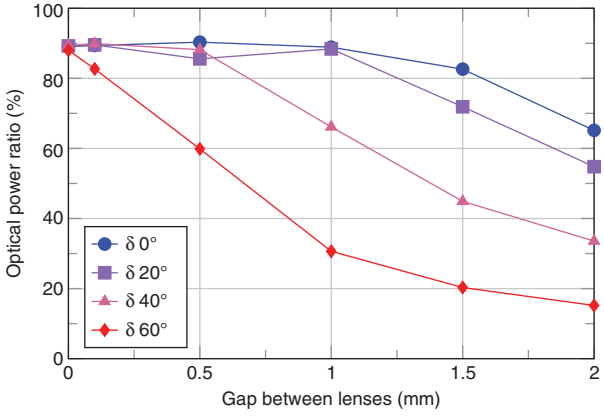

Figure 13: Optical power ratio of overlap area to reference spot over the gap between the lenses at different deflection angles. A VLPP with a semicircle RL and a radial constant gap between the lenses.

increased thickness of the RL. Because of the thicker lens, the exit point of the laser beam on the plane surface of the SL shifts toward its edge. Hence, a small part of the laser beam hits the side face of the SL instead of its plane surface. The angle of incidence on this side face is rotated by 90° to the plane surface, resulting in total internal reflection. Thus, this part of the laser beam is not deflected in the same direction and is missing in the spot evaluation. As already described for the effects of the eccentricity of the RL, this missing part of the laser beam leads to a shift in the centroid.

The conformity of the semi-axes shows a behavior similar to that of a VLPP described in Section 5 (see Figures 8 and 12). Still, a parasitic air lens is existent, but with a different range of focal lengths. Compared to the same LG, the focal length becomes shorter for small deflection angles, and greater deflection angles show the reverse effect. Therefore, the focal length of the parasitic air lens changes less over different LG and deflection angles.

Compared to the results in Figure 10, the optical power ratio illustrated in Figure 13 is more regular. This results from the lower influence of the parasitic air lens. Still, the simulation results are not completely satisfactory.

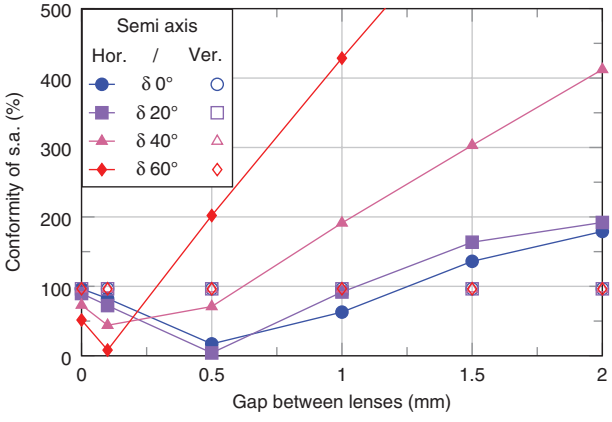

Figure 12: Conformity of semi-axes of the simulated spot ellipse to the reference spot ellipse over the gap between the lenses at different deflection angles. A VLPP with a semicircle RL and a radial constant gap between the lenses.

7 Summary and outlook

We present a new type of LiDAR sensor based on a variable lens pair prism. This system combines the principles of macro- and microscanners to obtain the advantages and eliminate most of the disadvantages of both system types. The concept of this new LiDAR sensor and the examination of the system performance by simulation are described. An approach to evaluate the spot shape and beam profile is introduced. The focus is the simulation and interpretation of the influences of important system parameters such as the gap between the lenses and deflection angle on the spot shape and beam profile.

One important result is that the gap between the lenses acts like a lens itself. As the gap is required to realise the system without abrasion, a way is investigated to reduce the effect of this parasitic air lens. An adjustable parameter for optimization is the radius of curvature of the lenses. Adjusting the curvature to obtain a radially constant gap between the lenses causes the relation between the deflection angle and the rotation angle to be independent of the LG. Additionally, the influences of the parasitic air lens on the spot shape become symmetric and

less intense. By increasing the thickness of the rotating lens, to get a semicircle in the cross section, the behavior of the VLPP, especially for large deflection angles, is improved.

Knowing the influence of the parasitic air lens allows a counteracting design of the laser beam before the VLPP. Thus, specified spot properties in the field of view may be achieved by adjusting the beam properties such as divergence and radius. At this, the beam properties should be designed for one selected LG so that they have the smallest possible deviations over the deflection angle range.

In conclusion, the introduced LiDAR sensor allows independent scans in horizontal and vertical direction, in which both scanning systems do not affect one another.

References

[1] J. Liu, Q. Sun, Z. Fan and Y. Jia, IEEE Optoelectronics Global Conference OGC, Shenzhen, China, 185–190 (2018).
[2] T. Fersch, R. Weigel and A. Koelpin, Proc. SPIE 10219, 1–12 (2017).
[3] H. Chen, J. Wang, P. Li, K. Li and J. Sun, in 'Proc. SPIE 6622, International Symposium on Photoelectronic Detection and Imaging 2007: Laser, Ultraviolet, and Terahertz Technology', (10 March 2008), SPIE 2008.
[4] X. T. Nguyen, V. L. Dinh, H.-J. Lee and H. Kim, IEEE Sens. J. 18, 559–568 (2018).
[5] B. Schwarz, Nat. Photonics 4, 429–430 (2010).
[6] D. Hall, Velodyne Acoustics Inc., US Patent US20100020306A1 (2010).
[7] D. Hall, Velodyne Acoustics Inc., US Patent US20110216304A1 (2011).
[8] H. Spies, Ingenieurbüro Spies GbR, Deutsches Patent DE102009035984A1 (2011).
[9] M. Köhler, Valeo Schalter und Sensoren GmbH, Deutsches Patent DE102012021831A1 (2014).
[10] J. Schenk and J. Nies, Valeo Schalter und Sensoren GmbH, Deutsches Patent DE102014111950A1 (2015).
[11] J. Nies, G. Lammel and J. Schenk, Valeo Schalter und Sensoren GmbH, Deutsches Patent DE102012020288A1 (2014).
[12] U. Lages and M. Kiehn, Valeo Schalter und Sensoren GmbH, Deutsches Patent DE102013012789A1 (2015).
[13] M. D. Adams, IEEE Sens. J. 2, 2–13 (2002).
[14] H. Spies, Ingenieurbüro Spies GbR, Deutsches Patent DE102005055572A1 (2007).
[15] C. Böhlau and J. Hipp, IBEO Automobile Sensor GmbH, Deutsches Patent DE10244641A1 (2004).
[16] P. Horvath, L. Lin and T. Schuler, Valeo Schalter und Sensoren GmbH, Deutsches Patent DE102014118054A1 (2016).
[17] P. Horvath, L. Lin and T. Schuler, Valeo Schalter und Sensoren GmbH, Deutsches Patent DE102014118055A1 (2016).
[18] OpticStudio®, Zemax (www.zemax.com).
[19] J. Eichler, L. Dünkel and B. Eppich, Laser Tech. J. 1, 63–66 (2004).

Matthias Baier
Robert Bosch GmbH, Chassis Systems Control, Herrenwiesenweg 24, 71701 Schwieberdingen, Germany; and Karlsruher Institut für Technologie, Lichttechnisches Institut, Engesserstraße 13, 76131 Karlsruhe Germany
Matthias.Baier2@bosch.com

Matthias Baier received his B.Eng. and M.Eng. degrees in Mechatronics from Heilbronn University of Applied Sciences, Germany. His master's thesis focused on integrating a MEMS mirror into a rotating macroscanner LiDAR sensor. Currently, he is a PhD student at the Karlsruhe Institute of Technology and at Robert Bosch GmbH. The subject of his PhD thesis is the development and investigation of a LiDAR sensor based on the combination of two state-of-the-art principles, micro- and macroscanners.

Jan Sparbert
Robert Bosch GmbH, Chassis Systems Control, Herrenwiesenweg 24, 71701 Schwieberdingen, Germany

Since 2016, Jan Sparbert is a systems engineer for an automotive LiDAR for highly automated driving at Robert Bosch GmbH, Abstatt, Germany. After his diploma in Electrical Engineering at the Christians-Albrechts-University in Kiel in 1996, he earned his PhD degree in the field of sensing and path planning for autonomous robots at the University of Ulm in 2002. He started at Bosch as a developer of sensor data fusion for assisted driving functions. In 2011, he switched to Bosch Corporate Research, where he worked on automated parking functions and performed scouting of new sensor technologies. There, he also prepared the development of an automotive LiDAR. He is expert in automotive sensors (LiDAR, radar, video, ultrasonic), their interaction with the perception, and their use in highly automated driving functions.

Cornelius Neumann
Karlsruher Institut für Technologie Lichttechnisches Institut, Engesserstraße 13 76131 Karlsruhe, Germany

Cornelius Neumann studied Physics and Philosophy at the University of Bielefeld, Germany. After his PhD, he worked for the automotive supplier Hella in the advanced development for automotive lighting. During his time at Hella, he was responsible for signal lighting, LED application, and acted as a director of the L-LAB, a laboratory for lighting and mechatronics in public-private partnership with the University of Paderborn, Germany. In 2009, he became Professor for Optical Technologies in Automotive and General Lighting and one of the two directors of the Light Technology Institute at the Karlsruhe Institute of Technology, Germany.